Materials Research Express

PAPER

Comparative study of the accuracy of characterization of thin films a-Si on glass substrates from their interference normal incidence transmittance spectrum by the Tauc-Lorentz-Urbach, the Cody-Lorentz-Urbach, the optimized envelopes and the optimized graphical methods

Materials Research Express

PAPER

Comparative study of the accuracy of characterization of thin films a-Si on glass substrates from their interference normal incidence transmittance spectrum by the Tauc-Lorentz-Urbach, the Cody-Lorentz-Urbach, the optimized envelopes and the optimized graphical methods

RECEIVED
19 October 2018

REVISED
14 November 2018

ACCEPTED FOR PUBLICATION
30 November 2018

PUBLISHED
12 December 2018

D A Minkov[1], G V Angelov[2], R N Nestorov[2], E Marquez[3], E Blanco[3] and J J Ruiz-Perez[4]

[1] College of Energy and Electronics, Technical University, Sofia, bul. Bulgaria 31, 2140 Botevgrad, Bulgaria
[2] Department of Microelectronics, Faculty of Electronics Engineering and Technologies, Technical University of Sofia, bul. Kliment Ohridski 8, Sofia 1000, Bulgaria
[3] Faculty of Science, Department of Condensed-Matter Physics, University of Cadiz, E-11510 Puerto Real, Cadiz, Spain
[4] Royal Institute and Observatory of the Navy, E-11100 San Fernando, Cadiz, Spain

E-mail: d.minkov@tu-sofia.bg

Keywords: thin film characterization, accuracy of characterization methods, comparative study

Abstract

Two RF magnetron sputtered a-Si thin films one of them several times thicker than the other are characterized by four methods. Since most literature data indicate presence of Urbach tails in the bandgap of a-Si, the two inverse synthesis methods based on the Tauc-Lorentz-Urbach model (TLUM) and the Cody-Lorentz-Urbach model (CLUM) are employed. It is clarified that the conventional envelope methods tend to overestimate the average thickness $\overline{d}_f$, and to underestimate the refractive index $n_f(\lambda)$ of the film. Therefore, the recently proposed optimized envelope method (OEM) and the optimized graphical method (OGM) are also employed. The accuracies of characterizations by these four methods are compared using a figure of merit (*FOM*), representing RMS deviation of the computed transmittance spe$_c$trum $T_c(\lambda)$ obtained using the computed film characteristics, from the measured transmittance spectrum $T(\lambda)$ of the specimen. The most accurate characterization of the thinner film is achieved by OEM, providing average film thicknesses $\overline{d}_f = 785$ nm, its thickness non-uniformity $\Delta d_f = 23.5$ nm, and $FOM = 2.63 \times 10^{-3}$. Although absorbance data for this film show that its band tails can be approximated as exponential (Urbach tails), the *FOM*s for the respective TLUM and CLUM characterizations are more than 38% larger than for OEM. The most accurate characterization of the thicker film is achieved again by OEM, providing $\overline{d}_f = 3939.1$ nm, $\Delta d_f = 53.1$ nm, and $FOM = 6.99 \times 10^{-3}$. TLUM and CLUM fail to characterize the thicker film with acceptable accuracy, which is attributed to presence of non-exponential band tail, revealed by absorbance data for this film. The superior performance of OEM is explained considering that it does not assume particular band tails shapes, unlike TLUM and CLUM, neither it uses existence of a wide spectral region of film transparency as an initial approximation, unlike OGM. This inherent flexibility, and the demonstrated here exceptional accuracy of OEM, make it suitable for very accurate characterization of different types of thin films, including doped films and organic films.

1. Introduction

The advances in microelectronics and nanoelectronics increase the necessity for accurate characterization of thin films. For optical characterization of dielectric or semiconducting thin film with average thickness $\overline{d}_f = [300,5000]$ nm is usually used a specimen consisting of the film deposited on a glass substrate. The normal

incidence transmittance spectrum $T(\lambda)$ of such specimen, scanned by UV–vis-NIR spectrophotometer, typically contains interference pattern with several apparent maxima and minima [1, 2].

The use of interference normal incidence transmittance spectrum (INITS) of the specimen ensures virtually identical distance which light with different wavelengths λ travels for one pass through the film. This is favorable for accurate characterization of the film, compared to reflectance methods such as the spectroscopic ellipsometry, especially for characterization of thicker films, due to the Snell's law and the reflectance measurement at oblique light incidence. Indeed, spectroscopic ellipsometry is usually used for characterization of films with average thickness $\overline{d}_f < 1500$ nm, whereas the accuracy of the characterization decreases with increasing $\overline{d}_f$ [3, 4].

The main spectrophotometric methods for characterization of thin film on glass substrate, from single INITS $T(\lambda)$, can be fundamentally divided in two groups based on: inverse synthesis, and envelopes [5]. In the inverse synthesis method (ISM) is employed a dispersion model containing at least one of the refractive index $n_f(\lambda)$ and the extinction coefficient $k_f(\lambda)$ of the film, and the unknown film characteristics are determined by fitting the computed INITS $T_c(\lambda)$ to the scanned $T(\lambda)$ [6, 7]. For characterization of amorphous materials by ISM, it should be considered that band tails exist in the bandgap of the material [8, 9], with presumably exponential distributions of electronic tail states, also known as Urbach tails [10, 11]. Accordingly, suitable dispersion models for ISM characterization of amorphous thin films are the Tauc-Lorentz-Urbach model and the Cody-Lorentz-Urbach models, where the product $n_f(E)k_f(E)$ is expressed by an exponential term for photon energies $E(\text{eV}) = 1239.8/\lambda(\text{nm})$ smaller than the bandgap energy E_g [12, 13].

In the envelope method (EM) is not employed a dispersion model of the film, i.e. EM is model free method, and the film characteristics are computed by using the upper envelope $T_+(\lambda)$ and the lower envelope $T_-(\lambda)$ of $T(\lambda)$, as well as the interference fringes equation [14, 15]. The tangential wavelengths λ_t correspond to the tangential points $T_+(\lambda_t)$ and $T_-(\lambda_t)$, where $T_+(\lambda)$ and $T_-(\lambda)$ are tangential to the smoothed transmittance spectrum $T_{sm}(\lambda)$ of the inherently noisy $T(\lambda)$. Since $T_+(\lambda_t)$ and $T_-(\lambda_t)$ depend on λ_t, which participates in the interference fringes equation, computation of accurate envelopes $T_+(\lambda)$ and $T_-(\lambda)$ is needed for accurate thin film characterization by EM [14–16].

Although the founding EM paper of Swanepoel [14] represents the single most cited method for characterization of thin films, according to Google Scholar data [17], that EM has a couple of notable deficiencies. More specifically, it assumes uniform film thickness d_f over the light spot, and uses transparency of the film in a wide spectral region as an initial approximation. Therefore, employing EM from [14] for characterization of a thin film, which is either non-uniform, or does not have a wide spectral region of transparency, can result in inaccurate characterization of the film.

The graphical method (GM) for characterization of a thin film on glass substrate uses the same pair of envelopes of $T(\lambda)$ as EM, and its distinction is the graphical determination of the lowest interference order m_1, corresponding to the longest wavelength extremum of $T(\lambda)$ [14]. Since both EM and GM from [14] do not account for the thickness non-uniformity of the film, neither for the light absorption in the substrate, these methods have been improved to account for these two phenomena, respectively in [18] and [19].

Furthermore, the algorithms of all of the above cited EMs and GMs contain subjectively chosen adjustable parameters, which can result in additional inaccuracy of the thin film characterization. More specifically, the EM algorithms from [15, 18] contain three such parameters, and the GM algorithm from [19] contains four such parameters.

The optimization of GM, proposed in [20], enables computing and employing optimized values of each of the four adjustable parameters of GM from [19], based on minimization of an error function (*EF*). However, both GM from [19] and the optimization of GM from [20] use transparency of the film in a wide spectral region as an initial approximation.

The optimization of EM, proposed in [21], enables computing and employing optimized values of each of the three adjustable parameters of EM from [18], by minimization of *EF*. Notably, the optimization of EM from [21] does not use transparency of the film as an initial approximation.

After completing the spectrophotometric characterization of a given thin film on a glass substrate, it is possible to compute $T_c(\lambda)$ of the specimen, from its already computed characteristics. Therefore, the root mean square deviation (*RMSD*) of $T_c(\lambda)$ from $T(\lambda)$ can be used as a figure of merit (*FOM*) of the accuracy of the characterization, whereas smaller value of *FOM* corresponds to more accurate characterization of the film [22]. This kind of study of the accuracy of spectrophotometric characterizations of ZrO2-MgO films with thickness of [310,430] nm has provided $FOM = [0.0056, 0.0068]$ for ISM characterizations, and $FOM = [0.0061, 0.0073]$ for EM characterizations [22].

The goal of the present study is to determine which methods can provide most accurate characterization of amorphous thin films from single INITS $T(\lambda)$ of the film on glass substrate specimen. Two a-Si thin films with dissimilar thicknesses are characterized. The film characterization methods used are: ISM with Tauc-Lorentz-Urbach dispersion (TLUM), ISM with Cody-Lorentz-Urbach dispersion (CLUM), optimization of EM (OEM),

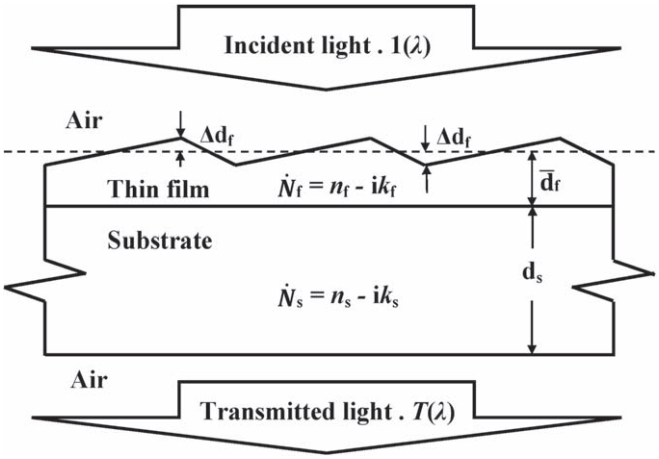

Figure 1. Layout of the specimen consisting of a thin film on a substrate with thickness $d_s \gg d_f$. $\dot{N}_f(\lambda) = n_f(\lambda)$—$ik_f(\lambda)$ and $\dot{N}_s(\lambda) = n_s(\lambda)$—$ik_s(\lambda)$ are the complex refractive indices of the film and the substrate. $T(\lambda)$ of the specimen is known.

and optimization of GM (OGM). These four methods are identified as most likely to provide accurate characterization of thin amorphous films.

2. Experimental details and theoretical background

The same two specimens and their respective transmittance spectra are used here, as in [20] and [21]. The specimen A038 consists of RF-magnetron sputtered a-Si film on a 0.9 mm thick Corning 7059 glass substrate, and the specimen A041 consists of another RF-magnetron sputtered a-Si film on a 3.28 mm thick Borofloat 33 glass substrate. The data for the refractive index $n_s(\lambda)$ and the extinction coefficient $k_s(\lambda)$ of the substrate are obtained by solving the system of two equations for the independently scanned transmittance $T_s(\lambda)$ and reflectance $R_s(\lambda)$ of the naked substrate, for each of the wavelengths of the scanned $T(\lambda)$ of the specimen. However, the derived and used here $n_s(\lambda)$ and $k_s(\lambda)$ are refined by slight smoothing and restricting $k_s(\lambda) \geqslant 0$, for all wavelengths of $T(\lambda)$, in comparison with those from [20] and [21]. $T(\lambda)$ of each of the specimens includes all integer wavelengths up to $\lambda = 2500$ nm, and the slit width is SW = 2 nm.

Both the substrate and the film are considered to be homogeneous, whereas $n_s(\lambda)$ and $k_s(\lambda)$ are independent from the position in the substrate, and $n_f(\lambda)$ and $k_f(\lambda)$ are independent from the position in the film. The film thickness $d_f = [\overline{d}_f - \Delta d_f, \overline{d}_f + \Delta d_f]$ is non-uniform over the spectrophotometric light spot, and $\Delta d_f > 0$ is the thickness non-uniformity of the film. A layout of the specimen and the spectrophotometric light used in this study is shown in figure 1.

In the considered here case of $n_f(\lambda) > n_s(\lambda) > 1$, the transmittance $T(\lambda)$ through the specimen depicted in figure 1 was formulated as [20, 21]:

$$T(\lambda) = \frac{1}{\delta_{f2} - \delta_{f1}} \int_{\delta_{f1}}^{\delta_{f2}} \frac{(\tau_{a,f}\tau_{f,s}\tau_{s,a})^2 x_f x_s}{a_1 - b_1 \cos(\delta_f) + c_1 \sin(\delta_f)} d\delta_f$$
$$= \frac{(\tau_{a,f}\tau_{f,s}\tau_{s,a})^2 x_f x_s}{(\delta_{f2} - \delta_{f1})\sqrt{a_1^2 - b_1^2 - c_1^2}} \left\{ \text{atan2}\left[\frac{(a_1 + b_1)\tan(\delta_{f2}) + c_1}{\sqrt{a_1^2 - b_1^2 - c_1^2}} \right] - \text{atan2}\left[\frac{(a_1 + b_1)\tan(\delta_{f1}) + c_1}{\sqrt{a_1^2 - b_1^2 - c_1^2}} \right] \right\} \quad (1)$$

in the case of $V_1 = \lambda^2/(2\pi n_s d_s \Delta\lambda) < 1$, where:

$$\tau_{a,f} = \frac{2}{\sqrt{(n_f + 1)^2 + k_f^2}}, \ \tau_{f,s} = 2\sqrt{\frac{n_f^2 + k_f^2}{(n_f + n_s)^2 + (k_f + k_s)^2}}, \ \tau_{s,a} = 2\sqrt{\frac{n_s^2 + k_s^2}{(n_s + 1)^2 + k_s^2}},$$

$$x_f = \exp(-4\pi k_f d_f/\lambda) = \exp(-\alpha_f d_f), \ \alpha_f = 4\pi k_f/\lambda, \ x_s = \exp(-4\pi k_s d_s/\lambda),$$
$$\delta_f = 2\pi n_f d_f/\lambda, \ \delta_{f1} = 2\pi n_f(\overline{d_f} - \Delta d_f)/\lambda, \ \delta_{f2} = 2\pi n_f(\overline{d_f} + \Delta d_f)/\lambda,$$

$$a_1 = 1 - (\rho_{a,f}\rho_{s,a}x_f x_s)^2 + \rho_{f,s}^2(\rho_{a,f}^2 x_f^2 - \rho_{s,a}^2 x_s^2),$$

$$b_1 = 2\rho_{a,f}\rho_{f,s}\rho_{s,a}x_f[\rho_{s,a}x_s^2 \cos\Delta_2 - \rho_{s,a}^{-1}\cos\Delta_1], \ c_1 = 2\rho_{a,f}\rho_{f,s}\rho_{s,a}x_f[\rho_{s,a}x_s^2 \sin\Delta_2 - \rho_{s,a}^{-1}\sin\Delta_1],$$

$$\rho_{a,f} = \sqrt{\frac{(n_f - 1)^2 + k_f{}^2}{(n_f + 1)^2 + k_f{}^2}},\ \rho_{f,s} = \sqrt{\frac{(n_f - n_s)^2 + (k_f - k_s)^2}{(n_f + n_s)^2 + (k_f + k_s)^2}},\ \rho_{s,a} = \sqrt{\frac{(n_s - 1)^2 + k_s{}^2}{(n_s + 1)^2 + k_s{}^2}},$$

$$\Delta_1 = \text{atan2}\left(\frac{2k_f}{n_f{}^2 + k_f{}^2 - 1}\right) + \pi + \text{atan2}\left[\frac{2(k_f n_s - k_s n_f)}{n_f{}^2 - n_s{}^2 + k_f{}^2 - k_s{}^2}\right],$$

$$\Delta_2 = \text{atan2}\left(\frac{2k_f}{n_f{}^2 + k_f{}^2 - 1}\right) + \pi - \text{atan2}\left[\frac{2(k_f n_s - k_s n_f)}{n_f{}^2 - n_s{}^2 + k_f{}^2 - k_s{}^2}\right],$$

The following approximated formula for the envelopes of $T(\lambda)$, at the tangential wavelengths λ_t, was obtained in [18]:

$$T_{(\pm)}(\lambda_t) = \frac{(\tau_{a,f_g}\tau_{f,s_g}\tau_{s,a_g})^2 x_f x_s}{\theta\sqrt{a_{1_g}{}^2 - b_{1_g}{}^2}}\ \text{atan2}\left[\frac{a_{1_g} \pm b_{1_g}}{\sqrt{a_{1_g}{}^2 - b_{1_g}{}^2}}\tan(\theta)\right] \tag{2}$$

where '+' from the '±' signs refers to $T_+(\lambda)$, and '−' refers to $T_-(\lambda)$, and:

$$\theta = 2\pi n_f \Delta d_f / \lambda_t$$

$$a_{1_g} = 1 - (\rho_{a,f_g}\rho_{s,a_g}x_f x_s)^2 + \rho_{f,s_g}{}^2(\rho_{a,f_g}{}^2 x_f{}^2 - \rho_{s,a_g}{}^2 x_s{}^2),$$

$$b_{1_g} = 2\rho_{a,f_g}\rho_{f,s_g}\rho_{s,a_g}x_f(\rho_{s,a_g}{}^{-1} - \rho_{s,a_g}x_s{}^2),$$

$$\tau_{a,f_g} = \frac{2}{n_f + 1},\ \tau_{f,s_g} = \frac{2n_f}{n_f + n_s},\ \tau_{s,a_g} = \frac{2n_s}{n_s + 1},$$

$$\rho_{a,f_g} = \frac{n_f - 1}{n_f + 1},\ \rho_{f,s_g} = \frac{n_f - n_s}{n_f + n_s},\ \rho_{s,a_g} = \frac{n_s - 1}{n_s + 1},$$

provided that: $V_2 = c_1/[(a_1+b_1)\tan(\theta)] \ll 1$, $V_3 = 2|(k_f n_s - k_s n_f)/(n_f^2 - n_s^2)| \ll 1$, $V_4 = [k_f/(n_f - 1)]^2 \ll 1$, $V_5 = [(k_f - k_s)/(n_f - n_s)]^2 \ll 1$, and $V_6 = [k_s/(n_s - 1)]^2 \ll 1$. Equation (2) was used in OGM [20], and in OEM [21], although written differently.

The computation of the envelopes is based on the algorithm from [23]. Therefore, in all considered cases in the present study, the envelopes are tangential to $T_{sm}(\lambda)$ at the tangent wavelengths λ_t, and pass through 'boundary points', 'convergence point', and 'supplementary points' [23]. Notably, by using $T_{sm}(\lambda)$ described in [23], each of the envelopes passes slightly internally with regard to $T(\lambda)$ in the vicinity of λ_t. However, it is also possible to extend $T_{sm}(\lambda)$ in the vicinity of any λ_t, whereas each of the envelopes touches externally $T(\lambda)$ at its respective $T(\lambda_t)$.

In this study are used several types of pairs of envelopes of the same $T(\lambda)$. For description of the envelope type are used one, two, or three subscripts. The first of these subscripts is '+' for an upper envelope, and '−' for a lower envelope. The second subscript can be '0' in case that the envelope is computed as in [23], i.e. it is either non-corrected, or corrected only for the slit width SW. Absence of a second subscript '0' and presence of a second subscript 'int' or 'ext' means, that the envelope is corrected differently. The last subscript can be 'int' in case that $T_{sm}(\lambda)$ is computed as in [23], which results in each of the envelopes passing slightly internally with regard to $T(\lambda)$ in the vicinity of its respective λ_t. The last subscript can be also 'ext' in case that $T_{sm}(\lambda)$ is extended in the vicinity of some λ_t, whereas each of the envelopes touches externally $T(\lambda)$ at all of its respective $T(\lambda_t)$.

Also in the algorithm from [23], both envelopes $T_+(\lambda)$ and $T_-(\lambda)$ are computed as being independent from the absorbance $x_s(\lambda)$ of the substrate. However, it is seen from equation (2) that $T_+(\lambda)$ and $T_-(\lambda)$ are proportional to $x_s(\lambda)$. Therefore, scaling $T_+(\lambda)$ and $T_-(\lambda)$ to reproduce the shape of $x_s(\lambda)$ might result in more accurate thin film characterization by OEM and OGM.

Besides, unlike the ISMs, the EMs use the interference fringes equation:

$$2n_f(\lambda_{ti})\overline{d}_f = m_i\lambda_{ti},\ \begin{cases} m_i \geqslant 1 - \textit{positive integer for } \lambda_{ti} \textit{ where } T_{sm}(\lambda_{ti}) = T_+(\lambda_{ti}) \\ m_i \geqslant 1/2 - \textit{positive half} - \textit{integer for } \lambda_{ti} \textit{ where } T_{sm}(\lambda_{ti}) = T_-(\lambda_{ti}) \end{cases} \tag{3}$$

where 'i' is a positive integer representing the number of the 'i-th' extremum of $T(\lambda)$ counted from its right end, m_i is the interference order of the 'i-th' extremum, and m_1 is the lowest interference order corresponding to the longest wavelength extremum of $T(\lambda)$. Moreover, it was shown in [24], that equation (3) is valid when:

$$V_7 = \frac{\text{atan2}\left(\frac{2k_f}{n_f{}^2 - 1}\right) + \text{atan2}\left[\frac{2(k_f n_s - k_s n_f)}{n_f{}^2 - n_s{}^2}\right]}{2\pi m_1} \ll 1. \tag{4}$$

Furthermore, since after a large number of reflections of light with wavelength λ at the boundary film/layer, it interacts non-coherently with newly incident light with the same wavelength λ in the film, the manifold reflected light will contribute non-coherently to $T(\lambda)$. Such light will contribute to decreasing $T_+(\lambda)$, and to

increasing $T_{-}(\lambda)$. The ratio $V_8(\lambda)$ between the non-coherent light contribution to $T(\lambda)$ and the coherent light contribution to $T(\lambda)$ was also derived in [24], whereas the condition for neglecting the non-coherent light contribution to $T(\lambda)$ is:

$$V_8 = \frac{(\rho_{a,f} x_f \rho_{f,s})^{2N_c}}{1 - (\rho_{a,f} x_f \rho_{f,s})^2} \ll 1, \tag{5}$$

and N_c is the number of double passes of light through the layer, during the known coherence time.

After both envelopes are determined, in the first parts of the OEM and the OGM algorithms are computed the average film thickness $\overline{d}_f$, the film thickness non-uniformity Δd_f, and the lowest interference order m_1 of $T(\lambda)$, by minimization of an error function EF [20, 21]. The EFs used here are SD/N_2 and $RMSD/N_2$, whose meaning is explained in [21].

In the second parts of the OEM and OGM algorithms is calculated $n_f(\lambda_{ti})$ for all tangential wavelengths λ_{ti} from equation (3). $k_f(\lambda_{ti})$ is computed by solving equation (1), applied to $T_{sm}(\lambda)$, using numerical integration with 100 steps. The spectral dependencies $n_f(\lambda)$ of the refractive index of the film is computed mainly by 'piecewise cubic Hermite polynomial interpolation' (PCHPI) of $n_f(\lambda_{ti})$, and $k_f(\lambda)$ is determined only by PCHPI of $k_f(\lambda_{ti})$ [23, 25].

At the end of a thin film characterization, by either of TLUM, CLUM, OGM, and OEM, are computed the film characteristics $\overline{d}_f$, Δd_f, $n_f(\lambda)$ and $k_f(\lambda)$. Thereafter, their respective transmittance spectrum $T_c(\lambda)$ is computed from equation (1), by using numerical integration with 100 steps, for every wavelength of the experimental spectrum $T(\lambda)$. The figure of merit FOM of the thin film characterization is defined as the root mean square deviation of $T_c(\lambda)$ from $T(\lambda)$:

$$FOM = RMSD(T_c, T) = \sqrt{\frac{\sum_{j=1}^{N_j} [T(\lambda_j) - T_c(\lambda_j)]^2}{N_j}} \tag{6}$$

where the summation is performed over all wavelengths of $T(\lambda)$ in the interval $[\lambda_{t1}, \min(\lambda_{ti})]$, and N_j is the number of such wavelengths. FOM from equation (6) represents the fitting error of $T_c(\lambda)$ to $T(\lambda)$ in the spectral region of quasi-transparency, weak, and medium absorption in the film, for the performed thin film characterization [2, 22].

3. Error considerations for thin film characterization methods

Some thin film characterization methods assume uniform film thickness d_f over the light spot [14, 26, 27], and other methods assume transparency of the film in a wide spectral region [12, 13, 28]. It is therefore useful to understand the influence of each of these two assumptions on the computed film characteristics.

In case that a method assuming uniform film thickness is used for characterization of a film with non-uniform film thickness, it should be taken into account that increasing either the film non-uniformity Δd_f or the extinction coefficient $k_f(\lambda)$ of the film results in decreasing the difference $T_{+}(\lambda)$ - $T_{-}(\lambda)$ between the envelopes of $T(\lambda)$ [21]. Therefore, characterization method assuming $\Delta d_f = 0$ reacts to the existence of film thickness non-uniformity $\Delta d_f > 0$ by overestimating $k_f(\lambda)$. Since the light transmission through the film is $\sim \tau_{a,f}^2 \tau_{f,s}^2 x_f \sim (n_f^2 + k_f^2) x_f$, and $x_f(\lambda) \sim 1$ in the interval $[\lambda_{t1}, \min(\lambda_{ti})]$, according to [29] and the formulae after equation (1), the overestimation of $k_f(\lambda)$ results in underestimation of $n_f(\lambda)$. Moreover, the underestimation of $n_f(\lambda_t)$ leads to overestimation of the average film thickness $\overline{d}_f$, as seen from equation (3).

Furthermore, in case that a method assuming existence of a wide spectral region with $k_f(\lambda) = 0$ is used for characterization of a film without such a region, the method reacts to $k_f(\lambda) > 0$ in this region by overestimating Δd_f. Since the difference $T_{+}(\lambda)$ - $T_{-}(\lambda)$ depends strongly on the parameter $\theta \sim n_f(\lambda) \Delta d_f$, defined in equation (2), overestimating Δd_f leads to underestimation of $n_f(\lambda)$. According to the previous paragraph, the underestimation of $n_f(\lambda)$ leads to overestimation of the average film thickness $\overline{d}_f$. The above conclusions correspond to the thin film characterization results described in [27, 30, 31].

Regarding the EMs, the considerations from the second paragraph of this section clarify that using the EM assuming uniform film thickness [14] for characterization of a film with non-uniform film thickness, results in overestimations of the average film thickness $\overline{d}_f$ and $k_f(\lambda_{ti})$, and underestimation of $n_f(\lambda_{ti})$. Furthermore, in the EM for non-uniform film thickness [18], Δd_f is computed explicitly from the equation (2) for $T_{+}(\lambda)$ and $T_{-}(\lambda)$, using existence of a wide spectral region with $k_f(\lambda) = 0$ as an initial approximation. Accounting for the last paragraph, using the EM from [18] for characterization of a film without a wide region with $k_f(\lambda) = 0$ leads to overestimation of $\overline{d}_f$, and underestimation of $n_f(\lambda_{ti})$. Notably, OEM from [21] does not assume uniform film thickness, neither it uses existence of a wide spectral region with $k_f(\lambda) = 0$ as an initial approximation.

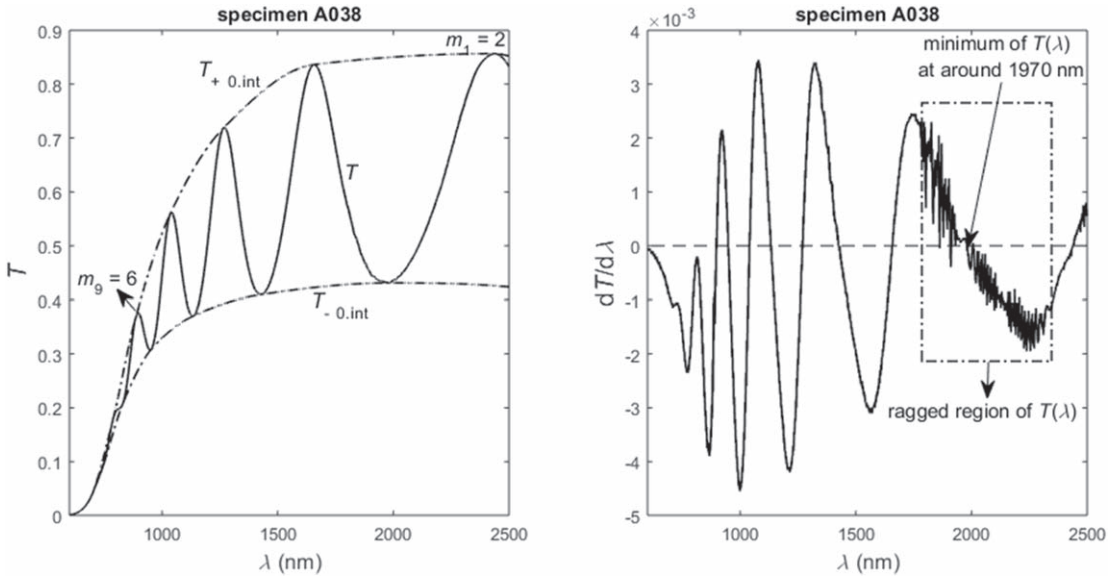

Figure 2. Left side: $T(\lambda)$ of the specimen A038, and its pair of envelopes $T_{+0.int}(\lambda)$ and $T_{-0.int}(\lambda)$ computed by using $T_{sm}(\lambda)$ as in [23]. Right side: The first derivative of $T(\lambda)$.

With respect to the GMs, the second paragraph of this section clarifies that using the GM assuming uniform film thickness [14] for characterization of a film with non-uniform film thickness, results in overestimations of the average film thickness $\overline{d}_f$ and $k_f(\lambda_{ti})$, and underestimation of $n_f(\lambda_{ti})$. Furthermore, in both GM for non-uniform film thickness [19] and OGM from [20], parameters θ_1 and T_{u-} are computed from equations for $T_+(\lambda)$ and $T_-(\lambda)$, similar to (2), using existence of a wide spectral region with $k_f(\lambda) = 0$ as an initial approximation. Notably, in this case Δd_f can be either overestimated or underestimated, since both θ_1 and T_{u-} are proportional to Δd_f.

Regarding TLUM and CLUM, it is taken into account that amorphous materials, and in particular a-Si and a-Si:H, are usually assumed to have Urbach tails [12, 13, 32]. However, there are also data about nonexponantial distributions of electronic tail states in a-Si:H [33]. Presence of such nonexponential distributions would result in nonexponential expression for the product $n_f(E)k_f(E)$ at $E < E_g$, and therefore in errors in the thin film characteristics computed by TLUM and CLUM in the interference region of $T(\lambda)$ of the respective specimen.

4. Results

4.1. Characterization of the film from the specimen A038

The scanned spectrum $T(\lambda)$ of the specimen A038 and its pair of envelopes $T_{+0.int}(\lambda)$ and $T_{-0.int}(\lambda)$ computed by using $T_{sm}(\lambda)$ as in [23], are shown in the left side of figure 2.

In the right side of figure 2 is shown the first derivative of $T(\lambda)$. Our analysis of the possible reasons for the existence of the ragged region of $T(\lambda)$ for $\lambda = [1770,2350]$ nm is based on data from [34–37], and indicates that it is most likely due to absorption by CO_2 and water vapor traces.

There is only one extremum of $T(\lambda)$ in this wavelengths interval, and its magnified surrounding is shown in the left side of figure 3. To compensate for the trace gas absorption, the transmittance spectrum is corrected to pass through the tops of $T(\lambda)$ only in this wavelengths interval, where the corrected transmittance spectrum $T_{cor}(\lambda)$ is considered to be identical to $T_{sm}(\lambda)$. No slit width correction of $T_{sm}(\lambda)$ [14] is performed for the specimen A038, since its maximum contribution to $T_{sm}(\lambda)$ is less than 3.9×10^{-5}.

Furthermore, both envelopes $T_{+int}(\lambda)$ and $T_{-int}(\lambda)$ are scaled to reproduce the shape of $x_s(\lambda)$, by introduction and use of their individual scaling factors. As always in this study, the envelopes are tangential to $T_{sm}(\lambda)$ at λ_t. Both, the non-corrected pair of envelopes $T_{+0.int}(\lambda)$ and $T_{-0.int}(\lambda)$, and the corrected pair of envelopes $T_{+int}(\lambda)$ and $T_{-int}(\lambda)$ are shown in the right side of figure 3, including also $T(\lambda)$ and $x_s(\lambda)$.

The film from A038 is characterized by each of the four discussed methods. Some of the computed results are presented in the upper part of table 1, for the non-corrected $T(\lambda)$ and its pair of envelopes $T_{+0.int}(\lambda)$ and $T_{-0.int}(\lambda)$; and in the lower part of table 1, for the corrected $T_{cor}(\lambda)$ and its corrected pair of envelopes $T_{+int}(\lambda)$ and $T_{-int}(\lambda)$.

It is seen from table 1 that $FOM = [4.50,6.91] \times 10^{-3}$ when using $T(\lambda)$. It is also seen that significantly lowered FOMs are computed for the characterizations by the CLUM, OEM, and OGM, when using the

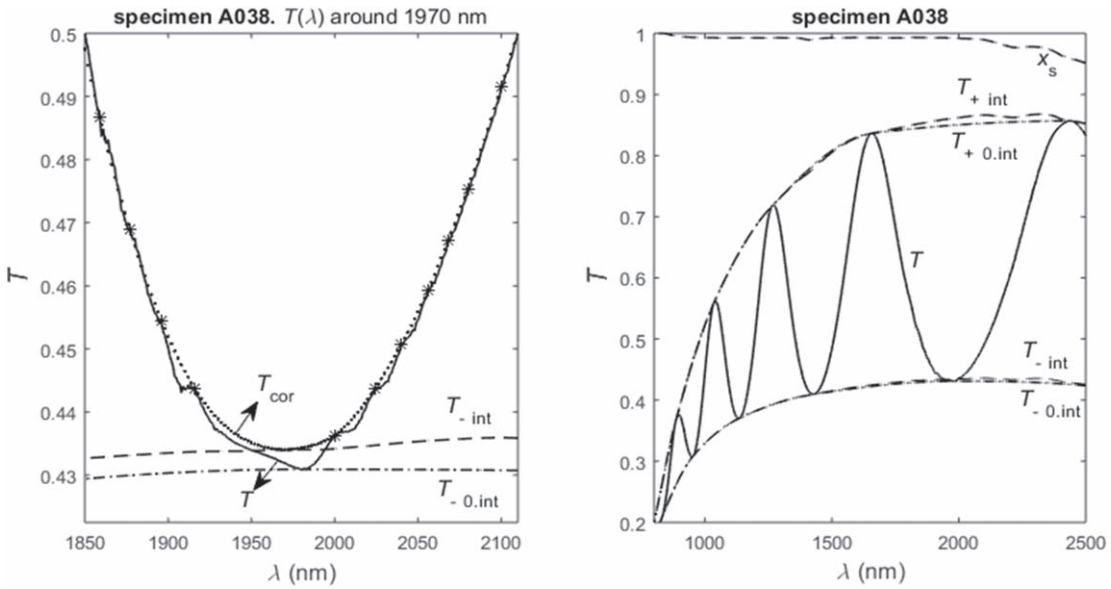

Figure 3. Left side: Zoomed image around the only influenced by trace gas minimum of $T(\lambda)$ of the specimen A038. The corrected $T_{cor}(\lambda)$ passes through the tops of $T(\lambda)$ for $\lambda = [1770,2350]$ nm. Right side: $T(\lambda)$, its non-corrected pair of envelopes $T_{+0.int}(\lambda)$ and $T_{-0.int}(\lambda)$, and its pair of envelopes $T_{+int}(\lambda)$ and $T_{-int}(\lambda)$ corrected for both the trace gas and the shape of $x_s(\lambda)$.

Table 1. Computed results from the characterizations of the a-Si film from the specimen A038. In the upper part of the table are shown data obtained from the non-corrected $T(\lambda)$ and its pair of envelopes $T_{+0.int}(\lambda)$ and $T_{-0.int}(\lambda)$. In the lower part of table are shown data obtained from the corrected $T_{cor}(\lambda)$ and its corrected pair of envelopes $T_{+int}(\lambda)$ and $T_{-int}(\lambda)$. The same $m_1 = 2$ is computed in all presented characterizations by OEM and OGM. The results with lowest *FOM* are highlighted in dark grey, and are regarded as the best characterization results.

Method	TLUM	CLUM	OEM		OGM	
distinctions of $T(\lambda)$ and its envelopes	$T(\lambda)$ is not corrected		The envelopes $T_{+0.int}(\lambda)$ and $T_{-0.int}(\lambda)$ are computed as in [23]			
error function (*EF*)			*RMSD/N*$_2$	*SD/N*$_2$	*RMSD/N*$_2$	*SD/N*$_2$
$\overline{d}_f$ (nm)	769	775	779.5	781.3	787.9	788.8
Δd_f(nm)	25	23.3	25.8	25.3	29.9	29.2
min(*EF*)			1.83×10^{-3}	0.459 nm	1.62×10^{-3}	0.438 nm
FOM for $\lambda = [\lambda_{t1}, \lambda_{t9}]$	4.50×10^{-3}	6.58×10^{-3}	5.42×10^{-3}	5.24×10^{-3}	6.90×10^{-3}	6.91×10^{-3}
distinctions of $T(\lambda)$ and its envelopes	$T(\lambda)$ is corrected for trace gas		the envelopes $T_{+int}(\lambda)$ and $T_{-int}(\lambda)$ are corrected for trace gas and x_s			
EF			*RMSD/N*$_2$	*SD/N*$_2$	*RMSD/N*$_2$	*SD/N*$_2$
$\overline{d}_f$ (nm)	769	783.5	785.0	785.7	789.1	789.5
Δd_f(nm)	25	24.3	23.5	23.1	29.5	29.2
min(*EF*)			1.23×10^{-3}	0.341 nm	9.74×10^{-4}	0.259 nm
FOM for $\lambda = [\lambda_{t1}, \lambda_{t9}]$	4.50×10^{-3}	4.30×10^{-3}	2.63×10^{-3}	2.64×10^{-3}	2.90×10^{-3}	2.91×10^{-3}

corrected transmittance spectrum $T_{cor}(\lambda)$ and its pair of envelopes $T_{+int}(\lambda)$ and $T_{-int}(\lambda)$. In this case, the lowest $FOM = 2.63 \times 10^{-3}$ is achieved for the characterization by OEM with *RMSD/N*$_2$. Amongst the other three characterization methods, the lowest $FOM = 2.90 \times 10^{-3}$ is achieved for the characterization by OGM with *RMSD/N*$_2$.

In figure 4 are shown the computed results for $n_f(\lambda)$ and $k_f(\lambda)$ obtained by the four characterization methods, using the computed data $m_1 = 2$, $\overline{d}_f$, and Δd_f providing their respective lowest *FOM*s from the lower part of table 1.

4.2. Characterization of the film from the specimen A041

Concerning the thin film from the specimen A041, our attempts to characterize it acceptably accurately by TLUM and CLUM have failed. $T(\lambda)$ of the specimen A041 has significantly smaller distances between its adjacent extrema, and narrower ragged looking tops, compared to these for the specimen A038. This shows that the film from the specimen A041 is significantly thicker than the film from the specimen A038. Correspondingly, even when the smoothing of $T(\lambda)$ of A041 is performed using a robust 'loess' with lower weight of the outliers and only five smoothing data points [25], both envelopes pass slightly internally with

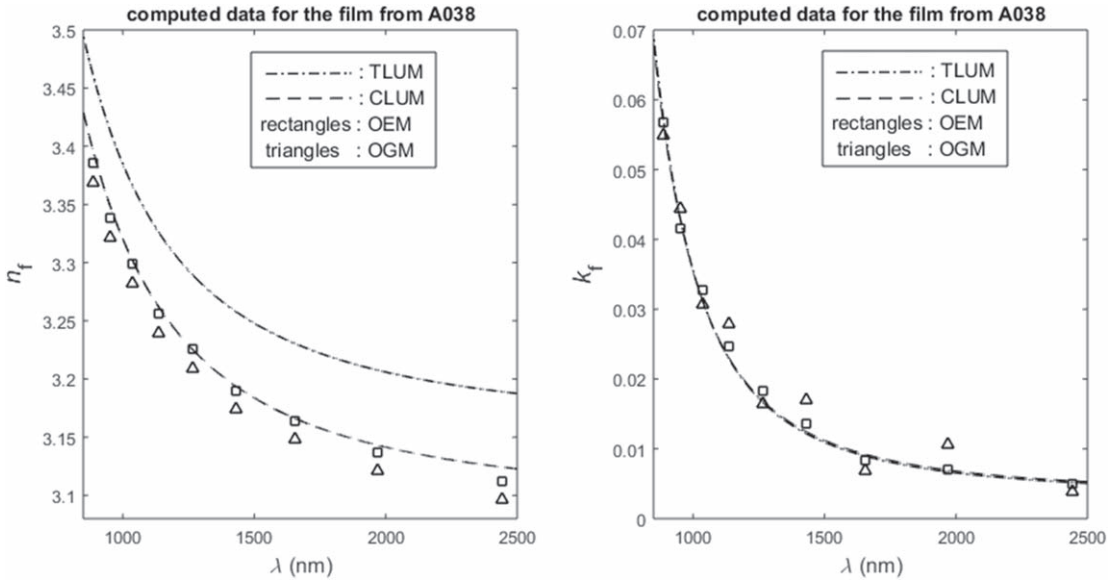

Figure 4. Computed dependencies $n_f(\lambda)$ and $k_f(\lambda)$ of the film from the specimen A038, obtained by the four characterization methods, using the computed data $m_1 = 2$, $\overline{d}_f$, and Δd_f providing their respective lowest *FOM*s from the lower part of table 1. Left side: $n_f(\lambda)$, and right side: $k_f(\lambda)$.

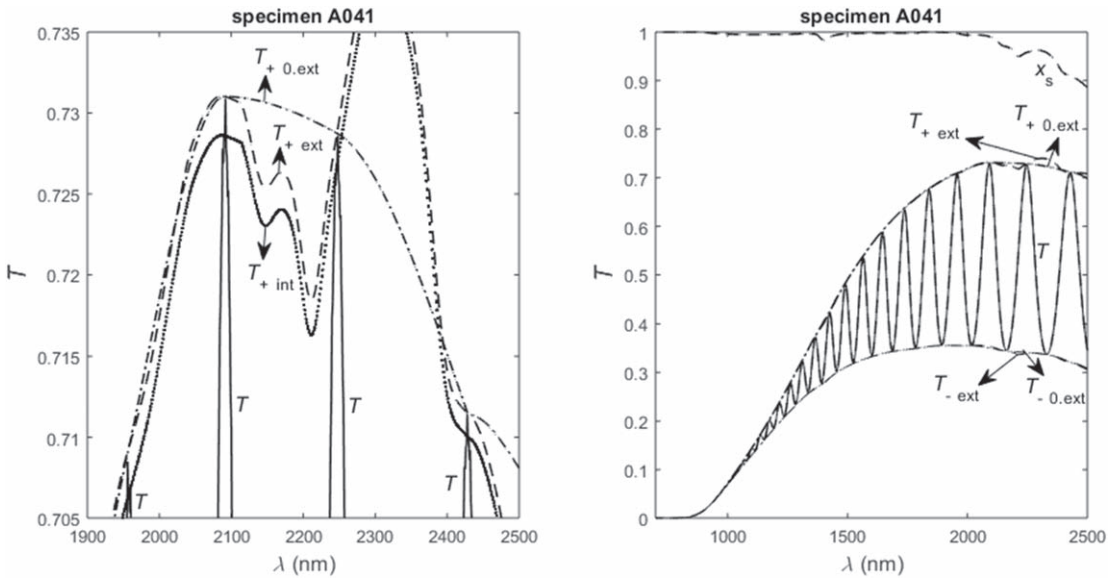

Figure 5. Left side: Zoomed image around the maxima of $T(\lambda)$ of A041 in the interval $\lambda = [1900,2500]$ nm. The envelope $T_{+0.ext}(\lambda)$ touches externally $T(\lambda)$ and is not corrected for $x_s(\lambda)$. The envelope $T_{+int}(\lambda)$ passes internally to $T(\lambda)$ and is corrected for $x_s(\lambda)$. The envelope $T_{+ext}(\lambda)$ passes externally to $T(\lambda)$ and is corrected for $x_s(\lambda)$. Right side: $T(\lambda)$ of A041, its pair of non-corrected for $x_s(\lambda)$ envelopes $T_{+0.ext}(\lambda)$ and $T_{-0.ext}(\lambda)$, its pair of corrected for $x_s(\lambda)$ envelopes $T_{+ext}(\lambda)$ and $T_{-ext}(\lambda)$, and $x_s(\lambda)$.

respect to $T(\lambda)$ in the vicinity of the tangential wavelengths [23]. Therefore, another smoothing of the same $T(\lambda)$ is also performed to touch it externally at its respective $T(\lambda_t)$.

Considering that the slit width SW is proportional to the film thickness [14], SW correction is always performed of the smoothed transmittance spectrum of A041, providing $T_{sm}(\lambda)$. The maximum contribution of this SW correction to $T_{sm}(\lambda)$ is 2×10^{-4}. Furthermore, both envelopes of $T(\lambda)$ of A041 can be scaled to reproduce the shape of $x_s(\lambda)$, as it was described for $T(\lambda)$ of A038.

A zoomed image around the maxima of $T(\lambda)$ of A041 in the wavelengths interval $\lambda = [1900, 2500]$ nm is shown in the left side of figure 5. There, the envelope $T_{+0.ext}(\lambda)$ is computed to touch externally $T(\lambda)$, and is not corrected for $x_s(\lambda)$. The envelope $T_{+int}(\lambda)$ passes internally to $T(\lambda)$ and is corrected for $x_s(\lambda)$. The envelope $T_{+ext}(\lambda)$ passes externally to $T(\lambda)$ and is corrected for $x_s(\lambda)$. $T(\lambda)$ of A041, its pair of non-corrected for $x_s(\lambda)$ envelopes $T_{+0.ext}(\lambda)$ and $T_{-0.ext}(\lambda)$, its pair of corrected for $x_s(\lambda)$ envelopes $T_{+ext}(\lambda)$ and $T_{-ext}(\lambda)$, and $x_s(\lambda)$ are

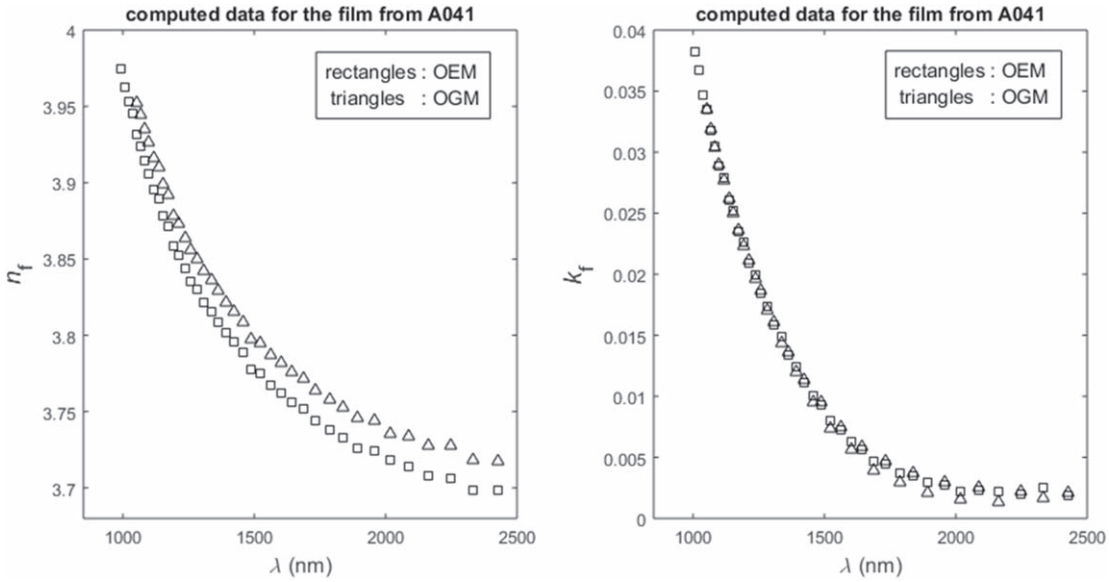

Figure 6. Computed results for the dependencies $n_f(\lambda_{ti})$ and $k_f(\lambda_{ti})$ of the film from the specimen A041, obtained using the data $m_1 = 12$, $\overline{d}_f$, and Δd_f highlighted respectively in dark grey and light grey in table 2. Left side: $n_f(\lambda_{ti})$, and right side: $k_f(\lambda_{ti})$.

Table 2. Computed results from OEM and OGM characterizations of the a-Si film from the specimen A041, by using the *EF* providing smaller *FOM* for a particular set of the pair of envelopes and the characterization method. All pairs of envelopes are SW corrected, and either of OEM or OGM computes $m_1 = 12$ in all presented characterizations. The results with lowest *FOM* are highlighted in dark grey, and are regarded as the best characterization results. The results with lowest *FOM* amongst the OGM characterizations are highlighted in light grey.

Method	OEM	OGM	OEM	OGM
envelopes distinctions	the envelopes $T_{+0.int}(\lambda)$ and $T_{-0.int}(\lambda)$ are computed as in [23]		the envelopes $T_{+0.ext}(\lambda)$ and $T_{-0.ext}(\lambda)$ touch externally $T(\lambda)$	
EF	SD/N_2	$RMSD/N_2$	SD/N_2	$RMSD/N_2$
$\overline{d}_f$ (nm)	3921.7	3896.9	3941.8	3918.4
Δd_f (nm)	55.0	52.6	53.0	50.7
min(*EF*)	0.561 nm	1.60×10^{-3}	0.513 nm	1.48×10^{-3}
FOM for $\lambda = [\lambda_{t1}, \lambda_{t35}]$	7.74×10^{-3}	8.17×10^{-3}	7.01×10^{-3}	7.36×10^{-3}
envelopes distinctions	the envelopes $T_{+int}(\lambda)$ and $T_{-int}(\lambda)$ are corrected for x_s		the envelopes $T_{+ext}(\lambda)$ and $T_{-ext}(\lambda)$ are external to $T(\lambda)$ and corrected for x_s	
EF	SD/N_2	SD/N_2	SD/N_2	SD/N_2
$\overline{d}_f$ (nm)	3918.6	3857.7	3939.1	3881.5
Δd_f (nm)	55.1	50.7	53.1	49.0
min(*EF*)	0.617 nm	0.419 nm	0.594 nm	0.421 nm
FOM for $\lambda = [\lambda_{t1}, \lambda_{t35}]$	7.75×10^{-3}	9.01×10^{-3}	6.99×10^{-3}	8.00×10^{-3}

shown in the right side of figure 5. Notably, the first derivative of $T(\lambda)$ of A041 does not contain a ragged part, unlike that of A038 from the right side of figure 2, which indicates that there is no need for its trace gas correction.

The film from the specimen A041 is characterized by OEM and OGM. Some of the computed results are presented in the upper part of table 2, for pairs of envelopes not corrected for $x_s(\lambda)$; and in the lower part of table 2, for pairs of envelopes corrected for $x_s(\lambda)$. Only results regarding the error function $RMSD/N_2$ or SD/N_2 providing the smaller *FOM* are shown, for a particular set of the pair of envelopes and the characterization method.

It is seen from table 2, that the lowest $FOM = 6.99 \times 10^{-3}$ is achieved for OEM characterization with *SD/N*2, when using the pair of envelopes $T_{+ext}(\lambda)$ and $T_{-ext}(\lambda)$ external to $T(\lambda)$ and corrected for x_s. In figure 6 are shown the computed results for $n_f(\lambda_{ti})$ and $k_f(\lambda_{ti})$ obtained by OEM and OGM, using the data $m_1 = 12$, $\overline{d}_f$, and Δd_f highlighted respectively in dark grey and light grey in table 2.

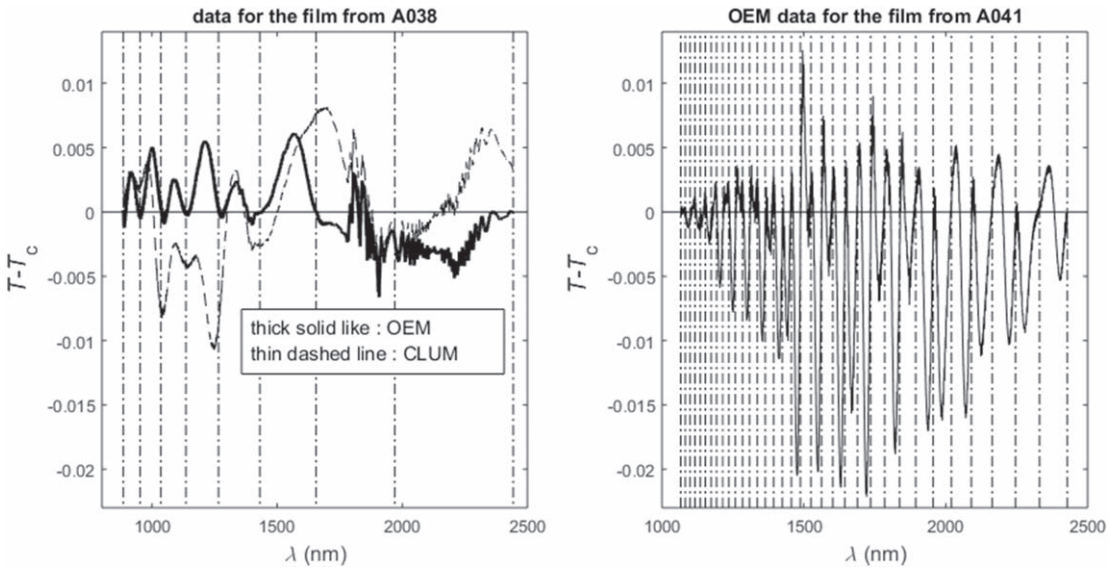

Figure 7. Spectral dependencies of the difference $T(\lambda)$ - $T_c(\lambda)$ for film characterizations by CLUM and OEM. Left side: for the film from the specimen A038, and right side: for the film from the specimen A041. In the computation of $T_c(\lambda)$ is used the respective set of the most accurate computed film characteristics m_1, $\overline{d}_f$, Δd_f, $n_f(\lambda)$ and $k_f(\lambda)$, for either of CLUM or OEM. The positions of λ_{ti} are represented by vertical dashed lines.

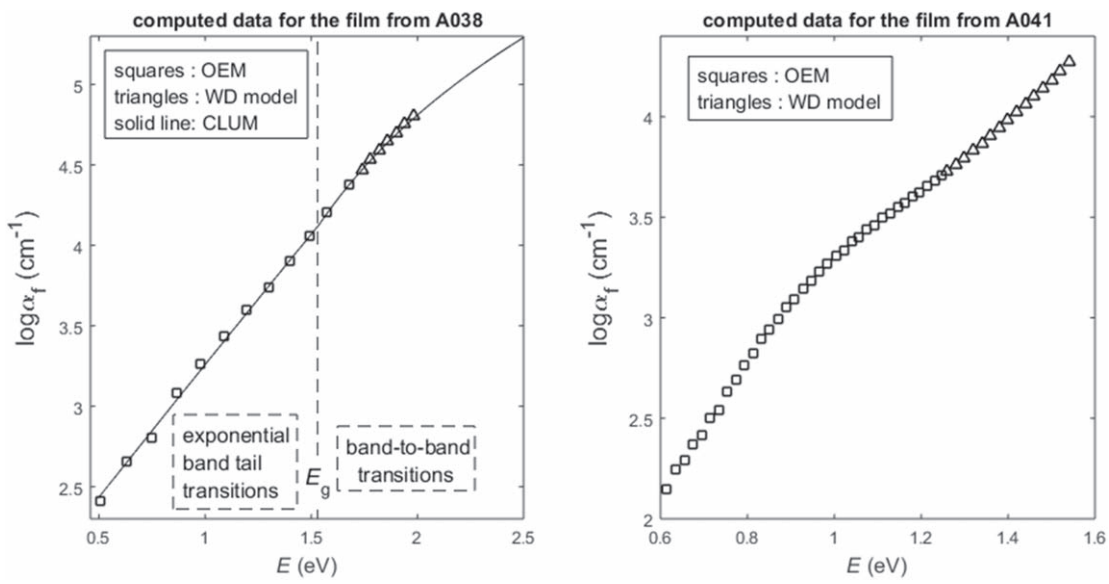

Figure 8. The dependence $\log\alpha_f(E)$ calculated from the most accurate data for $k_f(\lambda)$ computed by CLUM, OEM, and the WD model. Left side: for the film from the specimen A038, and right side: for the film from the specimen A041.

4.3. Computed results for the films from both specimens A038 and A041

It is seen from equation (6) that *FOM* is proportional to the difference $|T(\lambda) - T_c(\lambda)|$, where $T_c(\lambda)$ is computed from equation (1), by using the already computed characteristics of the film. The dependencies of the difference T - T_c on λ, for the films from the specimens A038 and A041, obtained by using CLUM and OEM and their respective sets of most accurate computed film characteristics m_1, $\overline{d}_f$, Δd_f, $n_f(\lambda)$ and $k_f(\lambda)$, are presented in figure 7.

For computation of $n_f(\lambda)$ for wavelengths below $\min(\lambda_{ti})$ is also used the Wemple-Di Domenico model (WD model), which is accepted to be valid for amorphous materials [38]. Once $n_f(\lambda)$ is known, its respective $k_f(\lambda)$ is computed by solving equation (1) for $T_{sm}(\lambda)$, using numerical integration with 100 steps. The dependence of $\log\alpha_f$ versus the photon energy E(eV) is calculated and shown in figure 8, by using the most accurate data for $k_f(\lambda)$ computed by either of CLUM, OEM, and the WD model, and their respective $\alpha_f(\lambda)$ defined in equation (1).

Table 3. Required and maximal most accurate computed values of the variables $V_1 > 0$ to $V_8 > 0$ from the left side of all of the inequalities, which should be fulfilled for accurate film characterization by OEM or OGM over the wavelengths interval [λ_{t1},min(λ_{ti})]. The computations are performed by using the respective sets of most accurate computed film characteristics m_1, $\overline{d}_f$, Δd_f, $n_f(\lambda)$ and $k_f(\lambda)$, for either of the films from the specimens A038 and A041.

Variable	V_1	V_2	V_3	V_4	V_5	V_6	V_7	V_8
required	< 1	$\ll 1$	$\ll 1$	$\ll 1$	$\ll 1$	$\ll 1$	$\ll 1$	$\ll 1$
A038	0.1696	8.59×10^{-3}	3.92×10^{-10}	9.10×10^{-4}	1.72×10^{-4}	2.34×10^{-3}	7.55×10^{-21}	7.47×10^{-21}
A041	0.0387	9.43×10^{-4}	7.12×10^{-3}	1.18×10^{-4}	1.69×10^{-4}	1.46×10^{-10}	1.53×10^{-4}	1.34×10^{-3}

To verify the degree of validity of the inequalities about the variables $V_1 > 0$ to $V_8 > 0$, which should be satisfied for accurate use of either OEM or OGM, their required and the maximal amongst their most accurate computed values are presented in table 3 for the films from the specimens A038 and A041.

5. Discussion

Since *FOM* represents the fitting error of the transmittance spectrum $T_c(\lambda)$ computed using the film characterization data, to the scanned transmittance spectrum $T(\lambda)$, smaller *FOM* implies more accurate film characterization. Besides, it is expected that characterization of films with larger thickness $\overline{d}_f$ and refractive index $n_f(\lambda)$ would result in larger *FOM*, since it is more difficult to fit accurately a curve to $T(\lambda)$ containing a larger number of extrema and having a larger difference $T_+(\lambda)$ - $T_-(\lambda)$ between its envelopes. Nevertheless, a comparison of the results from the upper part of table 1 and [22] shows that *FOM*s for the characterizations of the A038 film without corrections for trace gas and $x_s(\lambda)$ have similar values to *FOM*s from [22] for films with significantly smaller $\overline{d}_f$ and $n_f(\lambda)$. This is attributed to accounting for the film thickness non-uniformity Δd_f in each of the TLUM, CLUM, OEM and OGM employed here, unlike in [22].

A comparison between the *FOM*s for the A038 film, from the upper and the lower parts of table 1, indicates that the correction of $T(\lambda)$ for trace gas leads to decreasing the fitting error by about 35% for CLUM characterizations, while the fitting error is practically unchanged for TLUM characterizations. It is also seen that the correction of the pair of envelopes of $T(\lambda)$ for both trace gas and $x_s(\lambda)$ results in decreasing the fitting error by about 50% for OEM characterizations, and even more for OGM characterizations. The smallest *FOM* for the A038 film is achieved by using OEM with pair of envelopes $T_{+int}(\lambda)$ and $T_{-int}(\lambda)$ corrected for trace gas and $x_s(\lambda)$. Therefore, the respective $\overline{d}_f = 785.0$ nm and $\Delta d_f = 23.5$ nm are the most accurate thickness related data for the A038 film. Moreover, the fitting error for this OEM characterization is more than 38% smaller than for the respective TLUM and CLUM characterizations.

The studies of a-Si films [32, 39] have shown that both $n_f(\lambda)$ and $k_f(\lambda)$ have monotonically increasing negative first derivatives in the used here wavelength intervals. Similarly, it is seen from figure 4 that both $n_f(\lambda)$ and $k_f(\lambda)$ of the A038 film have monotonically increasing negative first derivatives, in case that the film is characterized by the OEM providing the smallest *FOM*.

The use of non-corrected pair of envelopes $T_{+0.int}(\lambda)$ and $T_{-0.int}(\lambda)$ results in erroneously elevated both $n_f(\lambda_t \sim 1970$ nm) and $k_f(\lambda_t \sim 1970$ nm), due to overestimating the difference $T_{+int}(\lambda_t \sim 1970$ nm) - $T_{-int}(\lambda_t \sim 1970$ nm) and underestimating $T_{-int}(\lambda_t \sim 1970$ nm), as seen from figure 3. Contrarily, the absence of erroneously elevated $n_f(\lambda_t \sim 1970$ nm) and $k_f(\lambda_t \sim 1970$ nm) in figure 4 indicates that the correction of $T(\lambda)$ for trace gas, illustrated in the left part of figure 3, has been performed properly. Furthermore, the correction of $T_{+int}(\lambda)$ and $T_{-int}(\lambda)$ to reproduce the shape of $x_s(\lambda)$ should lead to more accurate computation of all λ_{ti}, followed by more accurate calculations of $n_f(\lambda_{ti})$ from equation (3), and of $k_f(\lambda_{ti})$ from $T_{sm}(\lambda_{ti})$.

It is seen from table 1 and figure 4 that characterization of the A038 film by CLUM provides film characteristics differing from these obtained using OEM by 0.19% for $\overline{d}_f$, 0.34% for Δd_f, $\leqslant$ 0.39% for $n_f(\lambda)$, and $\leqslant$ 9.0% for $k_f(\lambda)$. The characterization of the A038 film by TLUT provides film characteristics differing from these obtained using OEM by 2.0% for $\overline{d}_f$, 6.4% for Δd_f, $\leqslant$ 2.1% for $n_f(\lambda)$, and $\leqslant$ 9.0% for $k_f(\lambda)$. These data indicate that the more than 38% smaller fitting error for the A038 film achieved by OEM, compared to TLUM an CLUM, leads mostly to more accurate computation of the extinction coefficient $k_f(\lambda)$.

It is also seen from table 1 and figure 4 that characterization of the A038 film by OGM provides film characteristics differing from these obtained using OEM as follows: overestimated $\overline{d}_f$ by 0.52%, overestimated Δd_f by 25.5%, underestimated $n_f(\lambda)$ by $\leqslant$ 0.49%, and oscillating behavior of $k_f(\lambda)$. According to comments from the third paragraph of section 3, the overestimation of $\overline{d}_f$ and Δd_f, and the underestimation of $n_f(\lambda)$ occur due to the use in OGM of the initial approximation of transparency of the film in a wide spectral region, although the A038 film is not transparent as seen from figure 4. For explanation of the behavior of $k_f(\lambda)$, it should be considered that $T_-(\lambda)$ increases significantly with decreasing $n_f(\lambda)$ and decreases with increasing $k_f(\lambda)$, while $T_+(\lambda)$ is almost independent from $n_f(\lambda)$ [14, 15]. Therefore, since $k_f(\lambda_t)$ is computed from $T_{sm}(\lambda_t)$ in this study

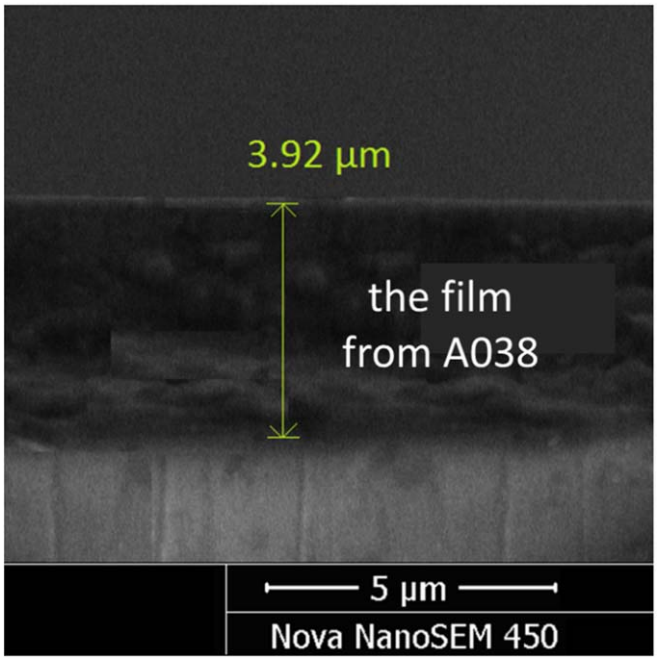

Figure 9. SEM image of a cross section of the film from the specimen A041. Reprinted from [21], Copyright (2018), with permission from Elsevier.

of OEM and OGM, the underestimation of $n_f(\lambda)$ in OGM leads to significant overestimation of $k_f(\lambda_t)$ for λ_t corresponding to the minima of $T_{sm}(\lambda)$, and to oscillating behavior of $k_f(\lambda_t)$.

Concerning the characterization of the A041 film by OEM and OGM, it is seen from the left side of figure 5 that both differences $T_{+0.ext}(\lambda)$ - $T_{+0.int}(\lambda)$ and $T_{+ext}(\lambda)$ - $T_{+int}(\lambda)$ between the envelopes touching externally and passing slightly internally with respect to $T(\lambda)$ can reach 0.0023. This relatively large value is a consequence of the large thickness of the A041 film, which results in narrow and ragged tops of $T(\lambda)$. Furthermore, it is seen from table 2 that *FOM* is always smaller when the envelopes touch externally $T(\lambda)$, compared to the envelopes passing internally to $T(\lambda)$, for each particular set of either corrected for $x_s(\lambda)$ or non-corrected for $x_s(\lambda)$ pair of envelopes and OEM or OGM characterization. These data show that more accurate characterization of the A041 film is always achieved by using a pair of envelopes touching externally $T(\lambda)$, than a pair of envelopes passing internally to $T(\lambda)$. However, a similar study of A038 film characterizations indicates that there is no notable difference between the *FOM*s in the cases of using a pair envelopes touching externally $T(\lambda)$ and a pair of envelopes passing internally to $T(\lambda)$. This is due to the small thickness of the A038 film, leading to wide and smooth tops of its respective $T(\lambda)$.

It is also seen from table 2 that the correction of the pair of envelopes for $x_s(\lambda)$ does not influence strongly the respective *FOM*s for the A041 film. Indeed, this correction does not influence strongly the computation of all λ_{ti}, due to the significantly narrower tops and valleys of $T(\lambda)$ for the A041 film, compared to $T(\lambda)$ for the A038 film, as seen from figure 3 and figure 5. Nevertheless, the smallest *FOM* amongst the characterizations of the A041 film is achieved by using OEM with the pair of envelopes $T_{+ext}(\lambda)$ and $T_{-ext}(\lambda)$ corrected for $x_s(\lambda)$, similarly to the A038 film characterizations. Therefore, the respective $\overline{d}_f = 3939.1$ nm and $\Delta d_f = 53.1$ nm are the most accurate thickness related data for the A041 film. For comparative purposes, SEM image of a cross section of the A041 film is shown in figure 9. Although the double-headed arrow from the SEM image indicates an approximate film thickness of 3920 nm, a careful observation shows that the average film thickness is slightly larger than 3920 nm.

Notably, the same lowest interference order $m_1 = 2$ is obtained in all OEM and OGM characterizations of the A038 film from table 1, and the same $m_1 = 12$ is obtained in all OEM and OGM characterizations of the A041 film from table 2. Considering the significant differences between the respective $\overline{d}_f$ and Δd_f of the A038 film and the A041 film, this indicates the capability of both OEM and OGM to determine accurately the lowest interference order m_1, for a variety of thin films.

The data from table 2 and figure 6 show that Δd_f and $\overline{d}_f$ are underestimated and $n_f(\lambda)$ is overestimated when using the OGM characterization of the A041 film with lowest *FOM*, compared to their respective values from the OEM characterization with lowest *FOM*. These results correspond to the comments from section 3. Furthermore, this OGM characterization provides oscillating behavior of $k_f(\lambda)$ in figure 6. Indeed, according to preceding considerations for the A038 film, since $k_f(\lambda_t)$ is computed from $T_{sm}(\lambda_t)$, the overestimation of $n_f(\lambda)$ in

this OGM characterization leads to significant underestimation of $k_f(\lambda_t)$ for λ_t representing the minima of $T_{sm}(\lambda)$.

The results from the left side of figure 7 indicate that $T_c(\lambda)$ computed using CLUM or TLUM differs notably from $T(\lambda)$ at the tangential wavelengths λ_{ti}, while the respective $T_c(\lambda)$ computed using OEM or OGM is quite close to $T(\lambda)$ at λ_{ti}. In fact, CLUM and TLUM essentially perform curve fitting of a computed transmittance spectrum to $T(\lambda)$, and such a fitting is relatively inaccurate around the extrema of an oscillating function. Moreover, in the studied here film characterizations by OEM and OGM, $k_f(\lambda_{ti})$ is computed from $T_{sm}(\lambda_{ti}) \cong T(\lambda_{ti})$, after all of the other thin film characteristics have been computed, which leads to $T_c(\lambda_{ti}) \cong T(\lambda_{ti})$.

Data about the bandgap energy $E_g = [1.3, 1.55]$ eV of a-Si films have been reported in [40, 41], and the more accurate CLUM characterization of the A038 film gives $E_g = 1.53$ eV. Besides, for Urbach tail transitions in studied a-Si film, the exponential behavior of $n_f(E)k_f(E)$ for $E < E_g$ should be dominated by $k_f(E)$, since it changes much faster than $n_f(E)$, as seen from figure 4 and figure 6. Therefore, the quasi-linear dependence of $\log\alpha_f(E)$ for $E < 1.53$ eV, from the left side of figure 8, indicates presence of quasi-Urbach tails for the A038 film. Furthermore, the good fit of the WD model data to the CLUM data for $E > 1.53$ eV, in the left side of figure 8, shows validity of the Wemple-Di Domenico model for the A038 film.

However, the dependence $\log\alpha_f(E)$ for $E < 1.53$ eV, from the right side of figure 8, is not linear. This indicates presence of non-exponential tail for the A041 film. Since both TLUM and CLUM assume presence of exponential tails, the presence of non-exponential tail can be the main reason for the failure of TLUM and CLUM to characterize accurately the A041 film.

A review of the data from table 3 shows that all of the used eight inequalities are fulfilled, in the OEM and OGM characterizations with minimal *FOM* of the A038 film and the A041 film. Indeed, V_1 is smaller than one, and the variables V_2 to V_8 do not exceed 0.01. Moreover, the obtained $V_7 < 1.6 \times 10^{-4}$ indicates that the interference fringes equation (3), used in both OEM and OGM, and not in CLUM and TLUM, is very accurate for either of the A038 film or the A041 film.

Furthermore, it is seen from table 3 that the contribution of the interference destructive non-coherent light interaction to $T(\lambda)$, represented as V_8, has a relatively large value of 1.34×10^{-3} for the A041 film. However, $V_8 < 8.1 \times 10^{-5}$ for $\lambda > 1160$ nm, whereas only this spectral region is used in the first part of the OEM and OGM characterizations of the A041 film. These data indicate that there is practically no interference destructive contribution to $T(\lambda)$, influencing the computations of m_1, $\overline{d}_f$, and Δd_f by OEM or OGM, for either of the A038 film or the A041 film.

6. Conclusions

Amorphous materials are usually considered to have exponential distributions of electronic tail states, also known as Urbach tails. Since TLUM and CLUM assume existence of Urbach tails, they are often used for characterization of amorphous thin films. Concerning the conventional envelope methods for thin film characterization, it is clarified here that they tend to overestimate the average film thickness $\overline{d}_f$, and to underestimate the refractive index $n_f(\lambda)$ of the film. Therefore, here are used their more complicated and more accurate versions OEM and OGM.

Since the accuracy of thin film characterization by all envelope methods depends on the accuracy of the pair of envelopes of $T(\lambda)$, computation of accurate envelopes is required for accurate thin film characterization by either of OEM or OGM. One improvement of the envelopes accuracy, comparative to the envelopes computation from [23], is achieved here by scaling both envelopes to reproduce the shape of $x_s(\lambda)$. Indeed, the characterization with lowest *FOM* is performed using a pair of envelopes corrected to reproduce the shape of $x_s(\lambda)$, for either of the two studied a-Si films. Second improvement of the envelopes accuracy, compared to [23], is the envelopes design to touch externally $T(\lambda)$ at the tangential points λ_{ti}. The results from table 2 indicate that this leads to increasing the film characterization accuracy for the thicker film specimen, whose extrema of $T(\lambda)$ are relatively narrow and ragged looking. Third improvement of the envelopes accuracy originates from the correction of $T(\lambda)$ to account for trace gas, revealed by the presence of a ragged part of the first derivative of $T(\lambda)$ for the specimen A038.

In the first parts of the OEM and OGM algorithms are computed the lowest interference order m_1, the average thickness $\overline{d}_f$, and the non-uniformity Δd_f of the film. In the second parts of the OEM and OGM algorithms are computed the refractive index $n_f(\lambda_{ti})$ from the interference fringes equation (3), and the extinction coefficient $k_f(\lambda_{ti})$ of the film from equation (1) applied to the smoothed spectrum $T_{sm}(\lambda_{ti})$, at the tangential wavelengths λ_{ti}. The dependencies $n_f(\lambda)$ and $n_f(\lambda)$ are obtained mainly by PCHPI of $n_f(\lambda_{ti})$ and $k_f(\lambda_{ti})$, respectively. The computed transmittance spectrum $T_c(\lambda)$ is obtained from equation (1) by using the already computed characteristics of the film. *FOM* calculated from equation (6) represents the fitting error of $T_c(\lambda)$ to $T(\lambda)$ in the spectral region of quasi-transparency, weak, and medium absorption in the film, for the performed

thin film characterization. Therefore, higher accuracy of a particular film characterization is revealed by lower *FOM* for this characterisation.

Most accurate amongst the 12 characterizations of the A038 film summarized in table 1, with lowest $FOM = 2.63 \times 10^{-3}$, is the OEM characterization using the pair of envelopes corrected for trace gas absorption and $x_s(\lambda)$. This characterization provides $\overline{d}_f = 785$ nm, $\Delta d_f = 23.5$ nm, as well as $n_f(\lambda_{ti})$ and $k_f(\lambda_{ti})$ shown in figure 4, which represent the most accurate characterization results for this thinner a-Si film. The respective dependence $\log\alpha_f(E)$ is presented in the left side of figure 8, including data from this OEM and CLUM characterizations, as well as WD model data. The agreement between all these data is good, whereas the CLUM characterization provides bandgap energy $E_g = 1.53$ eV. The quasi-linear behavior of $\log\alpha_f(E)$ for $E < E_g$ indicates presence of quasi-Urbach tails for the thinner a-Si film. Furthermore, the good fit of the WD model data to the CLUM data for $E > E_g$, in the left side of figure 8, demonstrates validity of the Wemple-Di Domenico model for the thinner a-Si film.

Most accurate amongst the 8 characterizations of the A041 film summarized in table 2, with lowest $FOM = 6.99 \times 10^{-3}$, is the OEM characterization using the pair of envelopes touching externally $T(\lambda)$ at λ_{ti}, and corrected for $x_s(\lambda)$ and for the slit width. This characterization provides $\overline{d}_f = 3939.1$ nm, $\Delta d_f = 53.1$ nm, as well as $n_f(\lambda_{ti})$ and $k_f(\lambda_{ti})$ shown in figure 6, which represent the most accurate characterization results for this thicker a-Si film. However, the respective dependence $\log\alpha_f(E)$, from the right side of figure 8, can not be approximated as linear for $E < 1.53$ eV, indicating presence of non-exponential tail, which can not be approximated as Urbach tail. Since both CLUM and TLUM failed to provide accurate characterization of the A041 film, this failure is attributed to the presence of non-exponential band tail for this thicker a-Si film.

Based on the above results, OEM provides the most accurate film characterizations for either of the thinner or the thicker a-Si films. This superior performance of OEM is explained considering that it does not assume particular band tails shapes, unlike TLUM and CLUM, neither it uses existence of a wide spectral region of film transparency as an initial approximation, unlike OGM. This inherent flexibility, and the demonstrated here exceptional accuracy of OEM, make it suitable for very accurate characterization of different types of thin films, including doped films and organic films.

ORCID iDs

D A Minkov https://orcid.org/0000-0003-1190-2598

References

[1] Stenzel O 2014 *Optical Coatings: Materials Aspects in Theory and Practice* (Heidelberg: Springer Series in Surface Sciences)
[2] Marquez E, Bernal-Oliva A M, Gonzalez-Leal J M, Alcon R P, Navarro J C and Minkov D 1999 Optical constants in the subgap region and vibrational behavior by far-infrared spectroscopy of wedge-shaped obliquely-deposited amorphous GeS2 films *Phys Scripta.* **60** 90–6
[3] Tompkins H G and Hilfiker J N 2015 *Spectroscopic Ellipsometry: Practical Application to Thin Film Characterization.* (New York: Momentum Press)
[4] Ogieglo W, Wormeester H, Eichhorn K J, Wessling M and Benes N E 2015 *In situ* ellipsometry studies on swelling of thin polymer films: A review *Prog. Polym. Sci.* **42** 42–78
[5] Poelman D and Smet P F 2003 Methods for the determination of the optical constants of thin films from single transmission measurements: A critical review *J. Phys. D: Appl. Phys.* **36** 1850–7
[6] Dobrowolski J A, Ho F C and Waldorf A 1983 Determination of optical constants of thin film coating materials based on inverse synthesis *Appl. Opt.* **22** 3191–200
[7] Macleod H A 2018 *Thin-film optical filters.* (Boca Raton: Taylor and Francis)
[8] Zanatta A R and Chambouleyron I 1996 Absorption edge, band tails, and disorder of amorphous semiconductors *Phys. Rev.* B **53** 3833–6
[9] Stewart K A, Yeh B S and Wager J F 2015 Amorphous semiconductor mobility limits *J. Non-Cryst. Solids* **432B** 196–9
[10] Ferlauto A S, Ferreira G M, Pearce J M, Wronski C R, Collins R W, Deng X and Ganguly G 2002 Analytical model for the optical functions of amorphous semiconductors from the near-infrared to ultraviolet: Applications in thin film photovoltaics *J. Appl. Phys.* **92** 2424–36
[11] Foldyna M, Postava K, Bouchala J, Pistora J and Yamaguchi T 2004 Model dielectric functional of amorphous materials including Urbach tail *Proc. SPIE* **5445** 301–5
[12] Jellison G E and Modine F A 1996 Parameterization of the optical functions of amorphous materials in the interband region *Appl. Phys. Lett.* **69** 371–3
[13] Guide to Using WVASE 32 2012 Spectroscopic Ellipsometry Data Acquisition and Analysis Software *LincolnJ. A. Woollam Co. Inc.*
[14] Swanepoel R 1983 Determination of the thickness and optical constants of amorphous silicon *J. Phys. E: Sci. Instrum.* **16** 1214–22
[15] Swanepoel R 1984 Determination of surface roughness and optical constants of inhomogeneous amorphous silicon films *J. Phys. E: Sci. Instrum.* **17** 896–903
[16] Jin Y, Song B, Jia Z, Zhang Y, Lin C, Wang X and Dai S 2017 Improvement of Swanepoel method for deriving the thickness and the optical properties of chalcogenide thin films *Opt. Express* **25** 440–51
[17] Swanepoel R 1983 Determination of the thickness and optical constants of amorphous silicon *J. Phys E: Sci. Inst.* **16** 1214
[18] Gonzalez-Leal J M, Prieto-Alcon R, Angel J A, Minkov D A and Marquez E 2002 Influence of substrate absorption on the optical and geometrical characterization of thin dielectric films *Appl. Opt.* **41** 7300–8

[19] Gavrilov G M 2016 Characterization of Chalcogenide Film on Substrate Specimens by the Graphical Method Using Accurate Refractive Index of the Substrate *Proc. of the XXV Int. Scientific Conf. Electronics (2016 Sept 12–14(Sozopol, Bulgaria: IEEE) p 203–6*
[20] Minkov D A, Gavrilov G M, Moreno J M D, Vazquez C G and Marquez E 2017 Optimization of the graphical method of Swanepoel for characterization of thin film on substrate specimens from their transmittance spectrum *Meas. Sci. Technol.* **28** 035202
[21] Minkov D A, Gavrilov G M, Angelov G V, Moreno G M D, Vazquez C G, Ruanod S M F and Marquez E 2018 Optimisation of the envelope method for characterisation of optical thin film on substrate specimens from their normal incidence transmittance spectrum *Thin Solid Films* **645** 370–8
[22] Jena S, Tokas R B, Thakur S and Sahoo N K 2013 Optical constants and thickness determination of thin films using envelope method and inverse synthesis method: a comparative study *Proc. of the 57th DAE Solid State Physics Symp. (2012 Dec 3–7(Mumbai, India: AIP) p 632–3*
[23] Gavrilov G M, Minkov D A, Marquez E and Ruano S M F 2016 Advanced computer drawing envelopes of transmittance spectra of thin film specimens. Intl. Adv *Res. J. Sci. Eng. Technol.* **3** 163–8
[24] Minkov D A Characterization of thin films and surface cracks in metals by electromagnetic methods and technologies *DSc thesis:* Avtoreferat; 2018; Technical University, Sofia, Bulgaria
[25] Fritsch F N and Carlson R E 1980 Monotone piecewise cubic interpolation *SIAM J. Numer. Anal.* **17** 238–46
[26] Birgin E G, Chambouleyron I and Martinez J M 1999 Estimation of optical constants of thin films using unconstrained optimization *J. Comput. Phys.* **151** 862–80
[27] Saleh M H, MMAG J, Bulos B N and Al-Daraghme TMF 2014 Determination of optical properties of undoped amorphous selenium (a-Se) films by dielectric modeling of their normal-incidence transmittance spectra *Appl Phys Res.* **6** 10–44
[28] Tatian B 1984 *Fitting Refractive-Index Data with the Sellmeier Dispersion Formula.* **23** 4477–85
[29] Minkov D A 1994 Flow-graph approach for optical analysis of planar structures *Appl. Opt.* **33** 7698–703
[30] Saleh M H, Ershaidat N M, Ahmad M J A and Bulos B N 2017 Jafar MMAG. Evaluation of spectral dispersion of optical constants of a-Se films from their normal-incidence transmittance spectra using Swanepoel algebraic envelope approach *Opt. Rev.* **24** 260–77
[31] Jafar M M A G, Saleh M H, Ahmad M J A, Bulos B N and Al-Daraghmeh TM. 2016 Retrieval of optical constants of undoped amorphous selenium films from an analysis of their normal-incidence transmittance spectra using numeric PUMA method *J Mater Sci-Mater El* **27** 3281–91
[32] Drabold D A, Li Y, Cai B and Zhang M 2011 Urbach tails of amorphous silicon *Phys. Rev.* B **83** 045201 1-6
[33] Brinza M, Emelianova E V and Adriaenssens G Y 2005 Nonexponential distributions of tail states in hydrogenated amorphous silicon *Phys. Rev.* B **71** 115209 1-11
[34] Intergovernmental Panel on Climate Change 2014 *Climate Change 2013 – The Physical Science Basis* (Cambridge: Cambridge University Press) (https://doi.org/10.1017/CBO9781107415324)
[35] (https://2.pvlighthouse.com.au/resources/courses/altermatt/The Solar Spectrum/Two mechanisms for atmospheric absorption of sunlight.aspx)
[36] Wright S A, Barton E J, Larkin J E, Moore A M, Crampton D and Simard L 2010 the IRIS team. The infrared imaging spectrograph (IRIS) for TMT: sensitivities and simulations *Proc. SPIE* **7735M** 1–9
[37] Hale G M and Querry M R 1973 Optical constants of water in the 200-nm to 200-μm wavelength region *Appl. Opt.* **12** 555
[38] Wemple S H and DiDomenico M 1971 Refractive-index behavior of amorphous semiconductors and glasses *Phys. Rev.* B **7** 3767–77
[39] Chittick R C 1970 Properties of glow-discharge deposited amorphous germanium and silicon *J. Non-Cryst. Solids* **3** 255–70
[40] Maley N and Lannin J S 1987 Influence of hydrogen on vibrational and optical properties of a-$Si_{1-x}H_x$ alloys *Phys. Rev.* B **36** 1146–51
[41] Berntsen A J M, van der Weg W F, Stolk P A and Saris F W 1993 Separating the effects of hydrogen and band-angle variation on the amorphous-silicon band gap *Phys. Rev.* B **48** 14656–8